

Computing Feasible Trajectories for an Articulated Probe in Three Dimensions^{*}

Ovidiu Daescu, Ka Yaw Teo[†]

Department of Computer Science, University of Texas at Dallas, Richardson, TX, USA.

Abstract

Consider an input consisting of a set of n disjoint triangular obstacles in \mathbb{R}^3 and a target point t in the free space, all enclosed by a large sphere S of radius R centered at t . An articulated probe is modeled as two line segments ab and bc connected at point b . The length of ab can be equal to or greater than R , while bc is of a given length $r \leq R$. The probe is initially located outside S , assuming an *unarticulated* configuration, in which ab and bc are collinear and $b \in ac$. The goal is to find a feasible (obstacle-avoiding) probe trajectory to reach t , with the condition that the probe is constrained by the following sequence of moves – a straight-line insertion of the unarticulated probe into S , possibly followed by a rotation of bc at b for at most $\pi/2$ radians, so that c coincides with t .

We prove that if there exists a feasible probe trajectory, then a set of *extremal* feasible trajectories must be present. Through careful case analysis, we show that these extremal trajectories can be represented by $O(n^4)$ combinatorial events. We present a solution approach that enumerates and verifies these combinatorial events for feasibility in overall $O(n^{4+\epsilon})$ time using $O(n^{4+\epsilon})$ space, for any constant $\epsilon > 0$. The enumeration algorithm is highly parallel, considering that each combinatorial event can be generated and verified for feasibility independently of the others. In the process of deriving our solution, we design the first data structure for addressing a special instance of circular sector emptiness queries among polyhedral obstacles

^{*}A preliminary version of this work was presented at the 31st Annual Canadian Conference on Computational Geometry.

[†]Corresponding author

Email addresses: ovidiu.daescu@utdallas.edu (Ovidiu Daescu),
ka.teo@utdallas.edu (Ka Yaw Teo)

in three dimensional space, and provide a simplified data structure for the corresponding emptiness query problem in two dimensions.

1. Introduction

In this paper, we address the three-dimensional (3D) version of the *articulated probe trajectory planning problem* introduced by Teo, Daescu, and Fox [20]. We are given a 3D workspace containing a set P of n interior disjoint triangular obstacles and a target point t in the free space, all located within a large sphere S of radius R centered at t (see Figure 1). An articulated probe is modeled as two line segments ab and bc joined at point b . Line segment ab has a length of R or greater, while bc has a fixed length $r \in (0, R]$. Line segment bc may rotate around b .

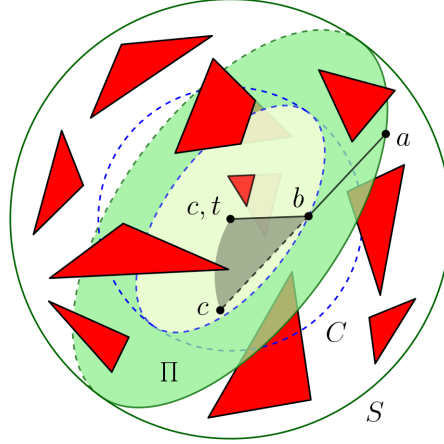


Figure 1: Articulated probe trajectory in 3D. After inserting line segment abc into sphere S , in order to reach target point t , line segment bc may be required to rotate from its intermediate position (dashed line segment) to its final position (solid line segment).

The probe is said to have an *unarticulated* configuration if line segments ab and bc are collinear, and $b \in ac$. Otherwise, the probe has an *articulated* configuration – that is, bc has been rotated around b , and bc is no longer collinear with ab .

The probe begins its trajectory in an unarticulated configuration outside sphere S . The unarticulated probe, represented by straight line segment abc , is at first inserted along a straight line into S . After completing the insertion, line segment bc may be rotated around point b up to $\pi/2$ radians in order to

reach the target point t . Hence, the final configuration of the probe could be either unarticulated or articulated. The *intermediate* configuration of the probe is the unarticulated configuration after the insertion and before the rotation. Without loss of generality, point a is assumed to be located on S after the insertion.

A *feasible* probe trajectory consists of an initial insertion of straight line segment abc into sphere S , possibly followed by a rotation of line segment bc around point b , such that point c ends at the target point t , while avoiding the obstacles in the process of insertion and rotation. The objective of the problem is to find a feasible probe trajectory, if one exists.

As illustrated in Figure 1, a feasible probe trajectory is planar – that is, its motion always lies in a plane Π passing through the target point t . Since line segment bc may only rotate as far as $\pi/2$ radians around point b , for any feasible probe trajectory, point b is the first (and only) intersection between line segment ab and the sphere C of radius r centered at the target point t . When line segment bc rotates around point b , the area swept by bc is a sector σ of a circle D in plane Π (i.e., a portion of a disk enclosed by two radii and a circular arc), where D is of radius r and centered at a point on sphere C . Circular sector σ always has an endpoint of one of its bounding radii located at the target point t .

Motivation

Besides its pointed relevance to robotics, the outlined problem arises particularly from planning for minimally invasive surgeries. In fact, surgical instruments that can be modeled by our simple articulated probe are already in clinical use (e.g., da Vinci EndoWrist by Intuitive Surgical), given their enhanced capability in reaching remote targets while circumventing surrounding critical structures [19]. In our problem setting, a human body cavity can be viewed as (a subset of) workspace S , and any critical organ/tissue can be represented by using a triangle mesh. Despite its importance and relevance, the problem has never been investigated in three dimensions from a theoretical viewpoint, and only a handful of results in two dimensions have been reported [8, 20].

Related work

The motion of a linkage or kinematic chain – that is, an assembly of rigid links and joints – has been investigated in many different aspects, including the basic geometric properties and topology of linkages (e.g., reconfiguration

and locked decision) [4, 7] as well as application-driven questions related to linkage design and motion planning [6, 13].

Approximation methods based on sampling [11, 14] and subdivision [5, 9, 22] are commonly used (and widely regarded as efficient) for motion planning involving complex multi-link robots with high degrees-of-freedom. However, a robotic linkage can often be associated with spatial (link or joint) constraints, resulting in a restricted free configuration space, which has proven to be challenging for inexact sampling-based algorithms to find valid solutions [21]. In addition, sampling- and subdivision-based approaches are only complete within their inherent limits – that is, probabilistically and resolution-wise, respectively.

In contrast to previous work on polygonal linkages, which are generally allowed to rotate unrestrictedly at their joints while moving from a start to a final configuration [6, 7, 13], our study is concerned with a simple articulated two-bar linkage subjected to a specific sequence of moves – namely, a straight-line insertion of the linkage followed by a rotation at its joint. Moreover, one of the links is assumed to have a length $\geq R$ (i.e., radius of spherical workspace S). Without resorting to approximation, we develop an exact geometric-combinatorial approach to solve the proposed path planning problem.

Teo, Daescu, and Fox [20] originally proposed the aforementioned trajectory planning problem in two dimensions (2D), and they presented an $O(n^2 \log n)$ -time, $O(n \log n)$ -space algorithm for finding a feasible trajectory amidst n line segment obstacles. The algorithm was based on computing extremal trajectories that are tangent to one or two obstacle vertices. In addition, they showed that, for any constant $\delta > 0$, a feasible trajectory of a clearance δ from the obstacles can be determined in $O(n^2 \log n)$ time using $O(n^2)$ space. These algorithmic approaches were also extended to the case of h polygonal obstacles, where a feasible trajectory can be found in $O(n^2 + h^2 \log n)$ time using $O(n \log n)$ space when no clearance is required, or $O(n^2)$ space otherwise.

Daescu and Teo [8] later addressed a variant of the trajectory planning problem where the length r of the end segment bc is not fixed. They demonstrated that, for any constant $\epsilon > 0$, the shortest length $r > 0$ for which a feasible trajectory exists can be determined in $O(n^{2+\epsilon})$ time using $O(n^{2+\epsilon})$ space, and at least one such trajectory can be reported with the same time/space complexity. The proposed algorithm can be extended to reporting all feasible values of r in $O(n^{5/2})$ time using $O(n^{2+\epsilon})$ space. In the same work,

Daescu and Teo also showed that, for a given r , the feasible solution space for the trajectory planning problem can be characterized by a simple-curve arrangement of complexity $O(k)$, and the arrangement can be constructed in $O(n \log n + k)$ time using $O(n + k)$ space, where $k = O(n^2)$ is the number of vertices of the arrangement.

Results and contributions

In this paper, we describe an algorithm that computes a feasible probe trajectory in 3D, if one exists, in $O(n^{4+\epsilon})$ time using $O(n^{4+\epsilon})$ space, for any constant $\epsilon > 0$. First, we prove that if there exists a feasible probe trajectory, then some *extremal* feasible trajectories must be present. An extremal trajectory is characterized by its intersections or tangencies with a combination of obstacle edges, vertices, and/or surfaces. Through careful case analysis, we show that these extremal trajectories can be represented by $O(n^4)$ combinatorial events. Our algorithm is based on enumerating and verifying these combinatorial events for feasibility. As an alternative, an $O(n^5)$ -time algorithm with $O(n)$ -space usage is achievable by performing a simple $O(n)$ -check on each of the $O(n^4)$ events.

The main new difficulty that arises in this study, when compared to the 2D case in [20], is the possibility that for an extremal trajectory in 3D, a segment of the probe may intersect an obstacle edge at an interior point, and an obstacle endpoint may be incident to the interior of the circular sector representing the area swept by the end segment bc of the probe. As a consequence, in order to address the 3D case, procedures and data structures different from those previously used in [20] are required, particularly for extremal trajectory computation and circular sector emptiness queries.

While deriving our solution approach, we develop the first data structure for solving a special case of the circular sector emptiness query problem in 3D, where the query circular sector has a fixed radius r and an endpoint of its arc located at fixed point t . We present a data structure of size $O(n^{4+\epsilon})$ for answering a query of the sort in $O(\log n)$ time. When mapped to the plane, this result yields a new data structure for solving the corresponding circular sector emptiness query problem in 2D. Our new \mathbb{R}^2 query data structure simplifies the two-part approach formerly proposed in [20] while maintaining the same time and space complexity. Sharir and Shaul [18] proposed a solution based on semialgebraic range searching for circular cap (i.e., portion of a circle cut off by a line and larger than a semidisk) emptiness queries in 2D. These circular sector emptiness queries, in 2D and 3D, are considered

to be of independent interest. To the best of the authors' knowledge, there has been no published data structure for general circular sector emptiness queries in 3D or even 2D.

The remainder of the paper is organized as follows. In Section 2, we prove the presence of extremal feasible probe trajectories. In Section 3, we describe an algorithm for computing extremal probe trajectories and verifying them for feasibility. We conclude in Section 4 by providing a summary of our results and a few related open questions.

2. Extremal feasible trajectories

In this section, we prove that if there exists a feasible probe trajectory, then a set of extremal feasible trajectories must also be present. We begin by defining a series of terminologies used in our ensuing discussion.

Let ℓ denote a line segment of the probe. In addition, let σ and γ denote a circular sector (i.e., area swept by bc , as previously described) and its arc, respectively. Let τ be a triangular obstacle of P in \mathbb{R}^3 , and let e denote an edge of τ . Without loss of generality, assume that τ is not co-planar with t , and ℓ is not parallel to e . Line segment ℓ may intersect e at an endpoint of e , an interior point of e , or none.

Definition 2.1 (Support vertex of ℓ). If ℓ intersects e at an endpoint p of e , then p is called a *support vertex* of ℓ .

Definition 2.2 (Support edge of ℓ). If ℓ intersects e at an interior point of e , then e is called a *support edge* of ℓ .

Thus, a *support* of ℓ can be either a support vertex or a support edge. Suppose, without loss of generality, that σ and e lie in different planes.

Definition 2.3 (Support vertex of σ). If σ contains an endpoint p of e , then p is a *support vertex* of σ .

Definition 2.4 (Support edge of γ). If γ is tangent to e at an interior point of e , then e is a *support edge* of γ .

Definition 2.5 (Support surface of γ). If γ is tangent to the surface of τ , then the surface is a *support surface* of γ .

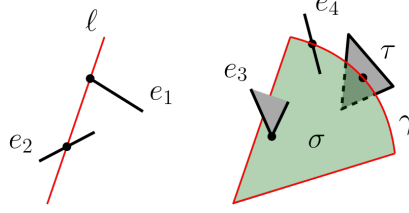


Figure 2: Support vertex, edge, and surface. An endpoint of edge e_1 is a support vertex of line segment ℓ . Edge e_2 is a support edge of ℓ . An endpoint of e_3 is a support vertex of circular sector σ . Edge e_4 supports circular arc γ at an interior point of e_4 . Triangle τ is a support surface of γ .

For an illustration of the various types of supports just described, see Figure 2.

A line segment is *extremal* (or *isolated*) with respect to a set of support vertices and edges if the line segment cannot be moved continuously while maintaining its intersections with these vertices and edges. Analogously, a probe trajectory is isolated by a set of supports if the trajectory cannot be altered without losing any of its supports. Note that the term “isolated” has the same meaning as “extremal,” and they will be used interchangeably hereafter.

Lemma 2.1. *Assume that a feasible **unarticulated** trajectory exists – that is, the unarticulated probe can be inserted into S to reach t while avoiding the obstacles (i.e., t can see to infinity without obstruction). Then, there exists an extremal feasible unarticulated trajectory such that the probe is isolated by either one support vertex or two support edges.*

Proof. Let T be a feasible probe trajectory such that its final configuration is unarticulated. Specifically, in the final configuration of the probe, abc is a straight line segment, and point c coincides with t .

Let Π be an arbitrary plane passing through t and containing line segment abc . Assume that plane Π intersects at least one triangular obstacle. Observe that such an arbitrary plane Π always exists; otherwise, workspace S must be free of obstacles. Let T' be the trajectory resulting from rotating T around t in plane Π until T intersects an obstacle edge at either i) an endpoint or ii) an interior point.

If the intersection occurs at an endpoint v of the obstacle edge, then we have a feasible trajectory T' that is isolated by a support vertex v (for t and v define a unique line).

On the other hand, suppose that T' intersects the obstacle edge at an interior point. Let e_1 denote the intersecting obstacle edge, and Ψ be the unique plane containing e_1 and t . When T' is rotated around t in plane Ψ until T' intersects an endpoint of e_1 or some obstacle edge e_2 , a new feasible trajectory T'' is obtained. If T'' intersects e_1 or e_2 at an endpoint, then T'' is isolated with respect to a support vertex. If T'' intersects e_2 at an interior point, then T'' is isolated with respect to two support edges (i.e., e_1 and e_2). \square

Lemma 2.2. *Assume that a feasible **articulated** trajectory exists – that is, the unarticulated probe can be inserted into S , and a subsequent rotation of bc around b can be performed to reach t , all while avoiding the obstacles. Then, there exists either*

- i) an extremal feasible unarticulated trajectory or*
- ii) an extremal feasible trajectory such that the probe assumes an articulated final configuration, and the trajectory is isolated with respect to at most four supports (edges, vertices, surfaces, or a combination of the three).*

Proof. Let T denote a feasible probe trajectory such that its final configuration is articulated. Namely, in the final configuration of the probe, ab and bc are not collinear, and point c coincides with t .

Let Π be the unique plane containing ab and t . Since the trajectory of the probe is planar (i.e., in plane Π), without loss of generality, assume that bc of T is rotated clockwise around b to reach t in plane Π . For ease of subsequent discussion, bc and bt (of an articulated trajectory) would be used to indicate line segment bc of the probe in its intermediate and final configurations, respectively.

A feasible trajectory T' can be obtained by rotating ab of T around b in clockwise direction in plane Π until either ab and bt become collinear or ab intersects an obstacle edge e_1 outside C . In the former case, T' has an unarticulated final configuration, and by directly applying Lemma 2.1, we obtain an extremal feasible unarticulated trajectory as a result. In the latter case, let T'' be the trajectory resulting from rotating bt of T' around t counter-clockwise in plane Π , while keeping ab intersecting e_1 , until either 1) bt or 2) ab intersects some obstacle edge e_2 . Trajectory T'' is feasible, and the proof is given in [20].

Case 1: bt intersects e_2 (inside C). Let p_1 be the intersection point between ab and e_1 . Let e_2' be the projection of e_2 onto the surface of sphere C from center t . Notice that e_2' is a circular arc on C , and point b of trajectory T'' must lie on e_2' as long as bt intersects e_2 (see Figure 3).

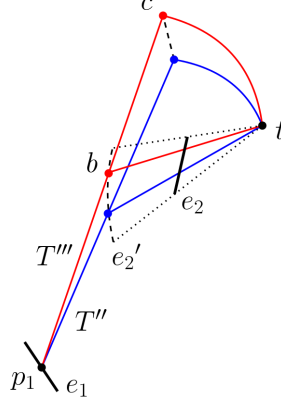


Figure 3: Illustration for Case 1.

Let σ_{bct} denote the minor circular sector (with a central angle $\leq \pi/2$ radians) bounded by radii bc and bt , and let γ_{ct} be the circular arc of σ_{bct} . Let point b of T'' be translated along e_2' in the direction such that the obtuse angle $\angle abt$ increases, while keeping ab intersecting e_1 at p_1 , until a) bt , b) bc , c) ab , d) σ_{bct} , or e) γ_{ct} intersects with an obstacle edge e_3 , f) γ_{ct} is tangent to the surface of some obstacle triangle, g) bt intersects with an endpoint of e_2 , or h) ab becomes collinear with bt . Let T''' denote the resulting trajectory, as depicted in Figure 3. Since T''' is obtained by simply perturbing T'' until the trajectory comes into contact with an obstacle (or $\angle abt$ reaches π radians), T''' is feasible.

Case 1(a): bt intersects e_3 . Note that two generic line segments and a point induce an incident line in 3D space. Since t is fixed and bt intersects two obstacle edges e_2 and e_3 , bt is isolated (and thus point b is fixed).

Let Ψ be the unique plane containing e_1 and b . As illustrated in Figure 4 Case 1(a), let T'''' be the trajectory obtained from rotating abc of T''' around b in plane Ψ in the direction such that the obtuse angle $\angle abt$ increases until i) bc , ii) ab , iii) σ_{bct} , or iv) γ_{ct} intersects with some obstacle edge e_4 , v) γ_{ct} is tangent to the surface of an obstacle triangle, vi) ab intersects an endpoint of

e_1 , or vii) ab becomes collinear with bt . Obviously, given that T''' is derived from T''' through a straightforward perturbation, T'''' is feasible.

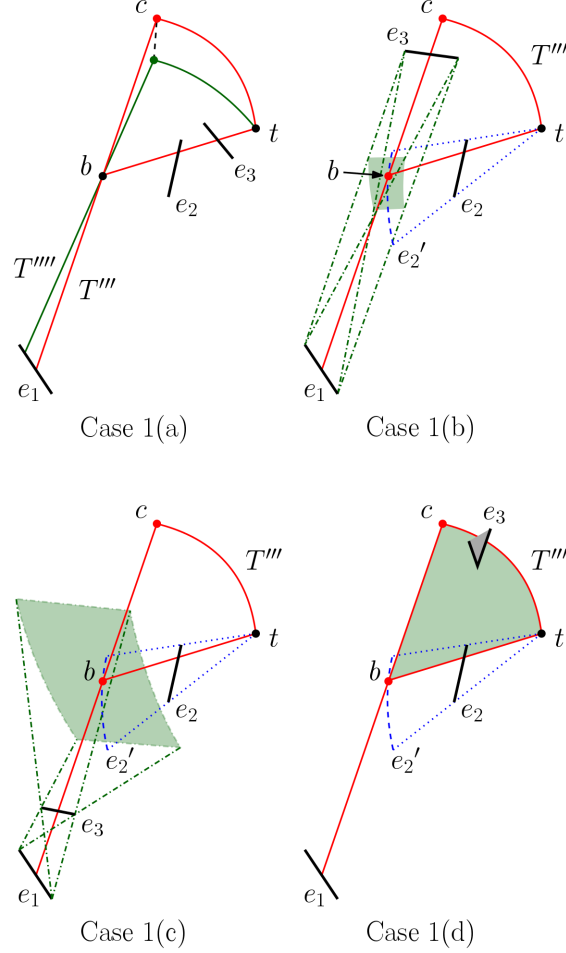


Figure 4: Illustrations for Cases 1(a)–(d).

Case 1(a)(i), (ii): bc or ab intersects e_4 . Since abc intersects two obstacle edges e_1 and e_4 (and b is fixed), abc is isolated. Thus, T'''' is an extremal feasible articulated trajectory.

Case 1(a)(iii): σ_{bct} intersects e_4 (at one of its endpoints). In 3D space, the intersection of two generic planes is a line. Since the plane containing σ_{bct} and the plane Ψ containing e_1 and b are fixed, their intersection line,

which supports abc , is fixed. Hence, T'''' is an isolated feasible articulated trajectory.

Case 1(a)(iv), (v): γ_{ct} intersects e_4 or is tangent to the surface of an obstacle triangle. The plane containing σ_{bct} is isolated, and so is abc (for more insight, see Cases 1(e) and (f) below). As a result, T'''' is an isolated feasible articulated trajectory.

Case 1(a)(vi): ab intersects an endpoint of e_1 . Since b is fixed, abc is isolated with respect to b and the intersected endpoint of e_1 . Thus, T'''' is an extremal feasible articulated trajectory.

Case 1(a)(vii): ab becomes collinear with bt . In this case, by directly applying Lemma 2.1, we claim that T'''' is an extremal feasible unarticulated trajectory.

Case 1(b): bc intersects e_3 . Note that ab intersects e_1 , and bc intersects e_3 . Let $P(e_1, e_3)$ be the set of points q for which there exists a line segment starting at e_1 , passing through q , and ending at e_3 . Let I be the intersection of $P(e_1, e_3)$, C , and e_2' (for an illustration, see Figure 4 Case 1(b), where I is indicated as the portion of the blue dashed line lying in the green shaded area). Notice that I is a circular arc on C . An isolated feasible trajectory can be obtained by translating point b of T''' along I in the direction such that the obtuse angle $\angle abt$ increases until i) bt , bc , ab , σ_{bct} , or γ_{ct} intersects with some obstacle edge e_4 , ii) γ_{ct} is tangent to the surface of an obstacle triangle, iii) bt , bc , or ab reaches an endpoint of its currently intersecting obstacle edge, or iv) ab becomes collinear with bt . The detailed analyses for Cases 1(b)(i)–(iv) (as well as similar others in the cases that follow) are omitted herein due to their similarity to those in Case 1(a).

Case 1(c): ab intersects e_3 . Notice that ab intersects two edges e_1 and e_3 . Assume, without loss of generality, that e_1 and e_3 are intersected by ab in the way depicted in Figure 4 Case 1(c). Let $P(e_1, e_3)$ be the set of points q for which there exists a ray starting at e_1 , passing through e_3 , and then through q . Let I be the intersection of $P(e_1, e_3)$, C , and e_2' . Note that I is a circular arc on C . Circular arc I is illustrated, in Figure 4 Case 1(c), as the portion of the blue dashed line lying in the green shaded area. An

isolated feasible trajectory can be obtained by moving point b of T''' along I in the direction that increases the obtuse angle $\angle abt$ until i) bt , bc , ab , σ_{bct} , or γ_{ct} intersects with an obstacle edge e_4 , ii) γ_{ct} is tangent to the surface of an obstacle triangle, iii) bt or ab reaches an endpoint of its currently intersecting obstacle edge, or iv) ab becomes collinear with bt .

Case 1(d): σ_{bct} intersects e_3 (at one of its endpoints). Observe, as shown in Figure 4 Case 1(d), that T''' can be made isolated if point b of T''' is further translated along e_2' , while keeping ab intersecting e_1 and maintaining the incidence between σ_{bct} and e_3 , until i) bt , bc , ab , σ_{bct} , or γ_{ct} intersects with some obstacle edge e_4 , ii) γ_{ct} is tangent to the surface of an obstacle triangle, iii) bt or ab reaches an endpoint of its currently intersecting obstacle edge, or iv) ab becomes collinear with bt . The resulting trajectory is feasible.

Case 1(e): γ_{ct} intersects e_3 . Let D be a sphere of radius r with center b located on sphere C . Note that D passes through t . Consider the scenario that D is tangent to obstacle edge e_3 . When D is rotated around t while maintaining its tangency to e_3 , the center b of D translates along a curve e_3' on C (see Figure 5).

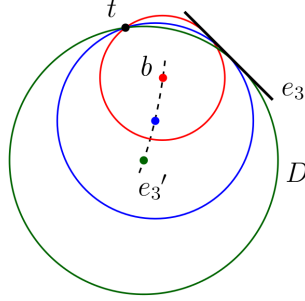


Figure 5: Illustration for Case 1(e). A top sectional view along the plane containing e_3 and t .

A plane can be defined by using two points on D and the center b of D . Consider a sphere D with center b on e_3' . Sphere D intersects t and is tangent to e_3 at a point p . Thus, we can define a plane Π_b containing t , p , and b , for any given point b on e_3' .

Notice that γ_{ct} is a circular arc on D originating at t , and γ_{ct} must be on the circle of intersection between D and Π_b , for some point b on e_3' . Since

e_2' and e_3' intersect at a point (i.e., point b on C), point b is fixed. As a result, plane Π_b is set, and so is the circle on which γ_{ct} lies. If Π_b does not contain e_1 , then abc is isolated. Otherwise, abc can be rotated around b , while continuing to intersect e_1 , until either ab or bc intersects an obstacle edge (or an endpoint of e_1). In the end of either scenario, an extremal feasible trajectory is obtained.

Case 1(f): γ_{ct} is tangent to the surface of an obstacle triangle. The analysis is similar to Case 1(e). Let τ denote the obstacle triangle to whose surface γ_{ct} is tangent. As D is rotated around t while remaining tangent to the surface of τ , the center b of D moves along a curve κ_τ on C . Given that e_2' and κ_τ intersect at a point, b is fixed. The same argument as in Case 1(e) immediately follows.

Case 1(g): bt intersects an endpoint of e_2 . Given that t is fixed, bt of T''' is isolated by its intersection with an endpoint of e_2 . A similar analysis as in Case 1(a) then follows.

Case 1(h): bc becomes collinear with bt . In this case, Lemma 2.1 is directly applicable, resulting in an extremal feasible unarticulated trajectory.

Case 2: ab intersects e_2 (outside C). Using similar arguments as given in Case 1, we can obtain an isolated feasible articulated trajectory such that i) ab intersects two edges, and ii) any of bt , bc , ab , σ_{bct} , and γ_{ct} are supported by at most two vertices, edges, and/or surfaces.

One may find some overlaps between Cases 1 and 2. On the whole, an extremal feasible articulated trajectory is characterized by its intersections (or tangencies) with at most four supports consisting of obstacle endpoints, edges, surfaces, or a combination of the three. This concludes the proof of Lemma 2.2. \square

3. Finding and validating extremal trajectories

Based on Lemmas 2.1 and 2.2, we can compute the set of extremal probe trajectories and verify them for feasibility. The algorithms and data structures required are discussed in this section.

3.1. Extremal feasible unarticulated trajectories

Let V and E denote the set of vertices and edges of the triangles of P , respectively. We compute the set R of rays, each of which i) originates at point t , ii) is either passing through a vertex of V or isolated with respect to two support edges of E , and iii) does not intersect any triangle of P in its interior. Each ray of R represents an extremal feasible unarticulated trajectory. Set R can be obtained by computing the visibility polyhedron from point t in $O(n^2)$ time using $O(n^2)$ space [15]. In fact, this approach yields all feasible unarticulated solutions, since the visibility polyhedron gives all unbounded rays from t to infinity (i.e., feasible unarticulated trajectories).

Lemma 3.1. *The set of all feasible unarticulated probe trajectories can be found in $O(n^2)$ time using $O(n^2)$ space.*

3.2. Extremal feasible articulated trajectories

We begin by computing the set of extremal articulated trajectories, which are characterized by $O(n^4)$ combinatorial events (see Lemma 2.2). As detailed next, these extremal articulated trajectories can be enumerated in $O(n^4)$ time either geometrically or algebraically.

3.2.1. Computing extremal articulated trajectories

Table 1 lists all the distinct cases of isolated articulated trajectories, each of which is indicated by the number of obstacle edges (i.e., support edges) intersected by line segments ab , bc , bt , and circular arc γ_{ct} , and the number of obstacle endpoints (i.e., support vertices) incident on the interior of circular sector σ_{bct} . Table 1 also provides, for each case, a brief description of the method (i.e., a sequence of geometric operations) and the worst-case time complexity for finding an extremal articulated trajectory. When describing the geometric operations in each case, obstacles edges are divided into those lying inside and outside C . Given that an obstacle edge may intersect C at most twice, an obstacle edge may be partitioned into at most three line segments.

Table 1: Extremal articulated trajectories.

Case	ab	bc	bt	σ_{bct}	γ_{ct}	Method	Time
1*	1	1	1	1		See main text in Section 3.2.1.	n^4
2	1	2	1			<ul style="list-style-type: none"> – For any three obstacle edges e_1, e_2, and e_3 (one outside C, and two inside or outside C), compute the projection (curve κ_1) of the hyperboloid that contains e_1, e_2, and e_3 on C. – For every obstacle edge e_4 inside C, compute its projection (curve κ_2) on C. – Compute the intersection of κ_1 and κ_2. 	n^4
3	1	1	2			<ul style="list-style-type: none"> – For any two obstacle edges e_1 and e_2 (one inside C, and the other inside or outside C), compute the projection (area A) of $P(e_1, e_2)$ on C. – For any two obstacle edges e_3 and e_4 inside C, compute the radial line segment s originating at t and intersecting e_3 and e_4, and determine the intersection point b between s and C. – Note that a distinct abc is given by a point b lying on A. 	n^4
Continued on next page.							

Case	ab	bc	bt	σ_{bct}	γ_{ct}	Method	Time
4	1		1	2		<ul style="list-style-type: none"> – For any two obstacle endpoints v_1 and v_2 (within distance $2r$ from t), compute the plane Π that contains v_1, v_2, and t. – For any obstacle edge e_1 outside C, compute the intersection of e_1 and Π. – For any obstacle edge e_2 inside C, compute the intersection of e_2 and Π. 	n^4
5	1		2	1		<ul style="list-style-type: none"> – For any two obstacle edges e_1 and e_2 inside C, compute the radial line segment s originating at t and intersecting e_1 and e_2, and determine the intersection point b between s and C. – For any obstacle endpoint v (within distance $2r$ from t), compute the plane Π that contains v, b, and t. – For any obstacle edge e_3 outside C, compute the intersection of e_3 and Π. 	n^4
6*	2		1	1		See main text in Section 3.2.1.	n^4
7*	2	1		1		See main text in Section 3.2.1.	n^4
Continued on next page.							

Case	ab	bc	bt	σ_{bct}	γ_{ct}	Method	Time
8	2	1	1			<ul style="list-style-type: none"> – For any three obstacle edges e_1, e_2, and e_3 (two outside C, and one inside or outside C), compute the projection (curve κ_1) of the hyperboloid that contains e_1, e_2, and e_3 on C. – For any obstacle edge e_4 inside C, compute its projection (curve κ_2) on C. – Compute the intersection of κ_1 and κ_2. 	n^4
9	2	2				For any four obstacle edges (two outside C , and two inside or outside C), compute the incidence lines induced by the four obstacle edges.	n^4
10	2		2			<ul style="list-style-type: none"> – For any two obstacle edges e_1 and e_2 outside C, compute the projection (area A) of $P(e_1, e_2)$ on C. – For any two obstacle edges e_3 and e_4 inside C, compute the radial line segment s originating at t and intersecting e_3 and e_4, and determine the intersection point b between s and C. – Note that a distinct abc is given by a point b lying on A. 	n^4
11	2			2		<ul style="list-style-type: none"> – For any two obstacle endpoints v_1 and v_2 (within distance $2r$ from t), compute the plane Π that contains v_1, v_2, and t. – For any two obstacle edges e_1 and e_2 outside C, compute their intersections with Π. 	n^4
Continued on next page.							

Case	ab	bc	bt	σ_{bct}	γ_{ct}	Method	Time
12	3	1				For any four obstacle edges (three outside C , and one inside or outside C), compute the incidence lines induced by the four obstacle edges.	n^4
13	3		1			<ul style="list-style-type: none"> – For any three obstacle edges e_1, e_2, and e_3 outside C, compute the projection (curve κ_1) of the hyperboloid that contains e_1, e_2, and e_3 on C. – For any obstacle edge e_4 inside C, compute its projection (curve κ_2) on C. – Compute the intersection of κ_1 and κ_2. 	n^4
14*	3			1		See main text in Section 3.2.1.	n^4
15	4					For any four obstacle edges outside C , compute the incidence lines induced by the four obstacle edges.	n^4
Continued on next page.							

Case	ab	bc	bt	σ_{bct}	γ_{ct}	Method	Time
16	1		1		1	<ul style="list-style-type: none"> – For any obstacle edge e_1 (within distance $2r$ from t), compute the curve κ_1 on which point b (i.e., the center of the sphere D tangent to e_1) lies. – For any obstacle edge e_2 inside C, compute its projection (curve κ_2) on C. – Compute the intersection point b between κ_1 and κ_2. – Compute the plane Π that contains t, b, and the point of intersection/tangency between e_1 and D. – For any obstacle edge e_3 outside C, compute the intersection of Π and e_3. – Assume that Π is not the same as the plane that contains b and e_3. 	n^3
17	1	1	1		1	<ul style="list-style-type: none"> – This is similar to Case 16 above with a different assumption at the end. – Assume that Π is the same as the plane that contains b and e_3. – For any obstacle edge e_4 inside or outside C, compute the intersection of Π and e_4. 	n^4
18	1		1	1	1	This can be thought of as Case 16 with an additional obstacle vertex supporting σ_{bct} (which does not contribute to additional extremal trajectories).	n^3
Continued on next page.							

Case	ab	bc	bt	σ_{bct}	γ_{ct}	Method	Time
19	1		2		1	This can be thought of as Case 16 with an additional obstacle edge intersecting bt (which does not contribute to additional extremal trajectories).	n^3
20	2	1			1	<ul style="list-style-type: none"> – For any three obstacle edges e_1, e_2, and e_3 (two outside C and one inside or outside C), compute the projection (curve κ_1) of the hyperboloid that contains e_1, e_2, and e_3 on C. – For any obstacle edge e_4 (within distance $2r$ from t), compute the curve κ_2 on which point b (i.e., the center of the sphere D tangent to e_4) lies. – Compute the intersection point b between κ_1 and κ_2. 	n^4
21	2		1		1	<ul style="list-style-type: none"> – This is similar to Case 16 with a different assumption at the end. – Assume that Π is the same as the plane that contains b and e_3. – For any obstacle edge e_4 outside C, compute the intersection of Π and e_4. 	n^4
22*	2			1	1	See main text in Section 3.2.1.	n^4

For conciseness, certain scenarios are omitted from Table 1 given their trivial nature, and they include those involving the isolation of a feasible articulated trajectory due to incidence of its line segment (i.e., ab , bc , or bt) with obstacle endpoints (i.e., support vertices). In addition, the cases in which γ_{ct} is tangent to the surface of an obstacle triangle are omitted due to their similarity to those where γ_{ct} is tangent to an obstacle edge.

Note that the set of extremal articulated trajectories, in all cases besides those denoted by * in Table 1, can be found by using a sequence of simple geometric operations (e.g., computing the intersection of two line segments

or planes). An extremal articulated trajectory in each of the five cases designated by * can be computed by using an algebraic-geometric approach. Given that these five cases are characteristically similar, as a demonstration, let us take a closer look at Case 1 from an algebraic point of view.

Recall that, in Case 1, ab intersects an edge e_1 , bt intersects an edge e_2 , and bc intersects an edge e_3 . In addition, σ_{bct} intersects an obstacle endpoint v . Let p (resp. q) denote the intersection between ab and e_1 (resp. bt and e_2).

Edges e_1 , e_2 , and e_3 can be expressed in parametric form as follows:

$$\begin{aligned} e_1 &= \{(1 - \lambda_1)u_1 + \lambda_1 v_1 : \lambda_1 \in \mathbb{R}, 0 \leq \lambda_1 \leq 1\} \\ e_2 &= \{(1 - \lambda_2)u_2 + \lambda_2 v_2 : \lambda_2 \in \mathbb{R}, 0 \leq \lambda_2 \leq 1\} \\ e_3 &= \{(1 - \lambda_3)u_3 + \lambda_3 v_3 : \lambda_3 \in \mathbb{R}, 0 \leq \lambda_3 \leq 1\} \end{aligned}$$

where $u_i, v_i \in \mathbb{R}^3$ are the two endpoints of edge e_i for $i = 1, 2, 3$. Analogously, line segments bt and pq can be defined, respectively, as

$$\begin{aligned} bt &= \{(1 - \lambda_{bt})b + \lambda_{bt}t : \lambda_{bt} \in \mathbb{R}, 0 \leq \lambda_{bt} \leq 1\} \\ pq &= \{(1 - \lambda_{pq})p + \lambda_{pq}q : \lambda_{pq} \in \mathbb{R}, 0 \leq \lambda_{pq} \leq 1\} \end{aligned}$$

where $b, p, q, t \in \mathbb{R}^3$. Since bt intersects e_3 ,

$$(1 - \lambda_{bt})b + \lambda_{bt}t = (1 - \lambda_3)u_3 + \lambda_3 v_3 \quad (1)$$

Furthermore, given that b must lie on a sphere of fixed radius r centered at t ,

$$(b - t) \cdot (b - t) = r^2 \quad (2)$$

where \cdot designates the dot product. Note that b must also be located on pq . Thus,

$$b = (1 - \lambda_{pq})p + \lambda_{pq}q \quad (3)$$

Since p and q are points on e_1 and e_2 , respectively,

$$p = (1 - \lambda_1)u_1 + \lambda_1 v_1 \quad (4)$$

$$q = (1 - \lambda_2)u_2 + \lambda_2 v_2 \quad (5)$$

The normal vector n of the plane Π defined by points t , b , and v can be expressed as

$$n = (b - t) \times (v - t)$$

where \times denotes the cross product. Since p (and thus q) must be in plane Π ,

$$\begin{aligned} n \cdot (p - t) &= 0 \\ [(b - t) \times (v - t)] \cdot (p - t) &= 0 \end{aligned} \tag{6}$$

At last, without loss of generality, t is assumed to be located at the origin:

$$t = (0, 0, 0) \tag{7}$$

Note that Equations 1, 3, 4, 5, and 7 are in vector form, and each of these equations yields three scalar equations (i.e., x , y , and z components). For instance, Equation 1 can be expressed, in scalar form, as

$$\begin{aligned} (1 - \lambda_{bt})b_x + \lambda_{bt}t_x &= (1 - \lambda_3)u_{3x} + \lambda_1v_{3x} \\ (1 - \lambda_{bt})b_y + \lambda_{bt}t_y &= (1 - \lambda_3)u_{3y} + \lambda_1v_{3y} \\ (1 - \lambda_{bt})b_z + \lambda_{bt}t_z &= (1 - \lambda_3)u_{3z} + \lambda_1v_{3z} \end{aligned}$$

Similarly, each of the vector variables b , t , p , and q consists of three scalar components (e.g., $b = (b_x, b_y, b_z)$). Hence, we have, in total, a system of 17 (scalar) parametric equations with 17 unknown (scalar) variables, which can be solved in constant time.

All in all, the worst-case running time for computing an extremal articulated trajectory is $O(n^4)$.

3.2.2. Validating extremal articulated trajectories

An extremal articulated trajectory is deemed feasible if and only if i) line segment ab and ii) circular sector σ do not intersect with any triangular obstacle in its interior. Checking for these scenarios can be reduced to the following two query problems – i) ray shooting query and ii) circular sector emptiness query.

Ray shooting queries

A ray shooting query among n interior disjoint triangles can be performed to determine whether a query line segment ab intersects with any triangular obstacle in its interior (i.e., whether a query line segment stabs through the interior of an obstacle triangle). According to de Berg et al. [3] and Pellegrini [16], such a query can be answered in $O(\log n)$ time using $O(n^{4+\epsilon})$ preprocessing time and space, for any constant $\epsilon > 0$. Alternatively, by using

the data structure proposed by Agarwal and Matousek [2], which provides a trade-off between space and time, a ray shooting query (amidst n triangles) can be answered in $O(n^{1+\epsilon}/m^{1/4})$ time using $O(m)$ storage and $O(m^{1+\epsilon})$ preprocessing time, for any $n \leq m \leq n^4$. By employing this fairly complex data structure, given that we have $O(n^4)$ queries, when $m = n$, we obtain $O(n^{3/4+\epsilon})$ time per query and $O(n^{19/4+\epsilon})$ total time.

Circular sector emptiness queries

In this section, we address a special instance of the circular sector emptiness query problem in 3D.

Given a set P of n triangles in \mathbb{R}^3 , preprocess it so that, for a query circular sector σ with a fixed radius r and an endpoint of its arc located at fixed point t , one can quickly determine whether σ intersects P .

Let Π be a plane passing through point t . We can parameterize Π by using two variables (I, Ω) (see Figure 6, where Π_0 is the plane with $I = 0$ and $\Omega = 0$).

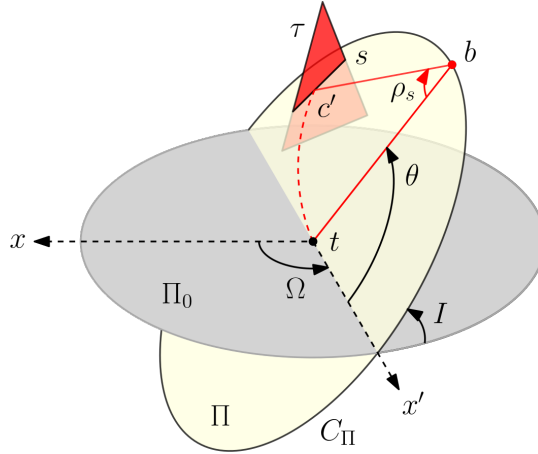


Figure 6: Characterization of ρ_s as function of θ in Π .

Let C_Π' be the circle in Π with radius $\sqrt{2}r$ and the center at t . Let τ be a triangle that intersects Π in a line segment s . Observe that a query circular sector σ in Π , as described above, can only intersect with τ if s intersects the interior of C_Π' .

Let C_Π denote the circle of radius r centered at t in Π . For any point $b \in C_\Pi$, let $\theta \in [0, 2\pi)$ be the angle of tb relative to the x -axis of Π (labeled as the x' -axis in Figure 6). Let bc' denote the farthest radius from bt , with respect to the circle of radius r centered at b in Π , before the minor circular sector bounded by radii bt and bc' intersects with s . Let ρ_s be the angle of bc' with respect to bt . Recall that line segment bc of the probe, after the insertion of the probe has completed, may only rotate up to $\pi/2$ radians in either direction in plane Π . Thus, $\rho_s \in [0, \pi/2]$. Here we consider ρ_s to be the clockwise angle from bt in plane Π . The other case can be handled symmetrically.

We fix plane Π (i.e., I and Ω) and proceed to characterize ρ_s as a function of θ . Two different cases are examined separately, depending on whether line segment s lies 1) inside C_Π or 2) outside C_Π and inside C_Π' . Note that a line segment s may intersect C_Π or C_Π' (or both). Since a line segment may intersect a circle at most two times, such a line segment can be partitioned into at most three line segments – one inside and two outside the circle – before proceeding with the following analysis.

Case 1: s lies inside C_Π . For brevity, the quarter-circular sector associated with a point b (i.e., the maximum possible area swept by bc to reach t), where the angle of tb relative to the x' -axis is θ , is henceforth referred to as the *quart-sector of θ* .

Let $\phi_{s,1}$, $\phi_{s,2}$, and $\phi_{s,3}$ be defined as follows (see Figure 7A). Angle $\phi_{s,1}$ is the smallest angle θ at which the circular arc of the quart-sector of θ intersects with s at one of its endpoints or an interior point. Angle $\phi_{s,2}$ is the smallest angle θ at which the radius bt of the quart-sector of θ intersects with s at one of its endpoints. Angle $\phi_{s,3}$ is the largest angle θ at which the radius bt of the quart-sector of θ intersects with s at one of its endpoints. In other words, as θ varies from 0 to 2π , $\phi_{s,1}$ and $\phi_{s,3}$ are the angles θ at which the quart-sector of θ first and last intersects with s , respectively.

For a line segment s lying inside C_Π , as shown in Figure 7, we are only concerned with computing ρ_s for $\theta \in [\phi_{s,1}, \phi_{s,2}]$, given that $\theta \in [\phi_{s,2}, \phi_{s,3}]$ is infeasible due to intersection of bt with s , and $\rho_s = \pi/2$ for $\theta \in [0, \phi_{s,1}] \cup [\phi_{s,3}, 2\pi)$.

Let α_s be the angle θ of the intersection point between C_Π and the supporting line of s . For $\theta \in [\phi_{s,1}, \phi_{s,2}]$, $\rho_s(\theta)$ can be represented by a piecewise continuous curve, which consists of at most two pieces, corresponding to two

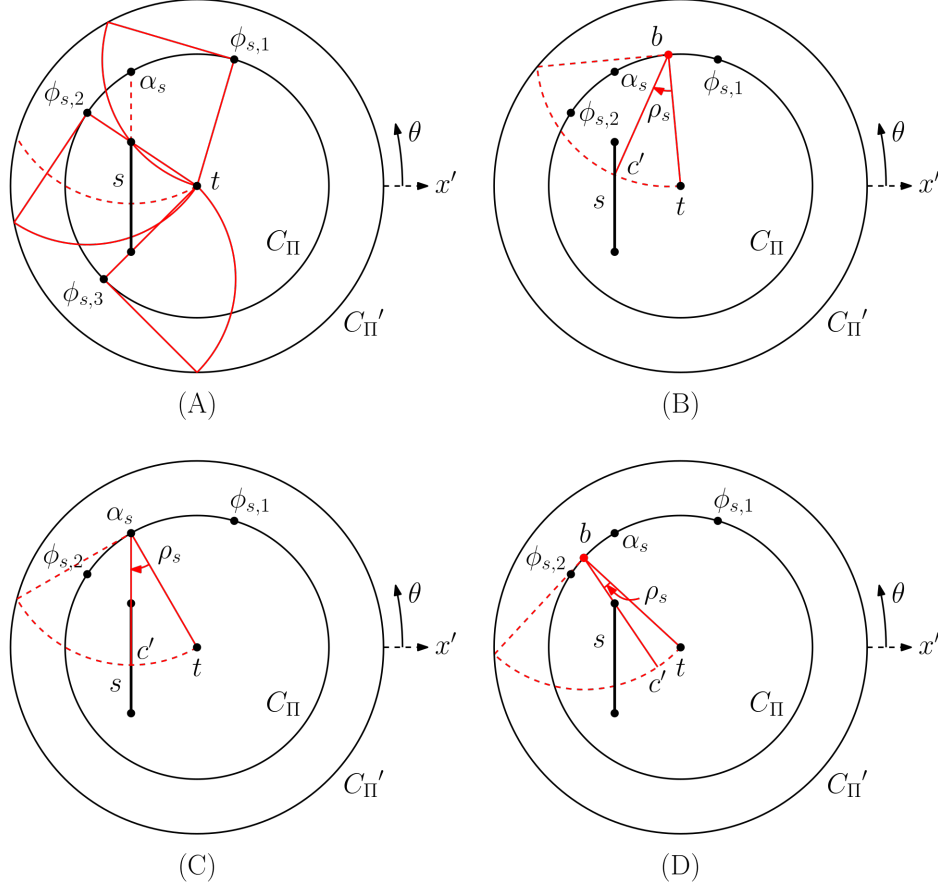


Figure 7: (A) Characterizing $\rho_s(\theta)$ for $\theta \in [\phi_{s,1}, \phi_{s,2}]$ in Case 1. Illustrations for $\rho_s(\theta)$ when (B) $\phi_{s,1} < \theta < \alpha_s$, (C) $\theta = \alpha_s$, and (D) $\alpha_s < \theta < \phi_{s,2}$, respectively.

sub-intervals $[\phi_{s,1}, \alpha_s]$ and $[\alpha_s, \phi_{s,2}]$. Note that if $\phi_{s,1} \leq \alpha_s$, then the curve of $\rho_s(\theta)$ has two pieces; otherwise, $\rho_s(\theta)$ is composed of one single piece.

Let c' denote the intersection point between line segment s and the circle D_{Π} of radius r centered at b . In the case of $\phi_{s,1} \leq \alpha_s$, for any $\theta \in [\phi_{s,1}, \alpha_s]$, as depicted in Figure 7B, $\rho_s(\theta)$ is given by the angle between bt and bc' . For any $\theta \in [\alpha_s, \phi_{s,2}]$ (and $\theta \in [\phi_{s,1}, \phi_{s,2}]$ in the case of $\phi_{s,1} > \alpha_s$), $\rho_s(\theta)$ is the angle between bt and bc' , where bc' intersects an endpoint of s at an interior point of bc' (see Figure 7D). Observe that $\rho_s(\theta) = 0$ when $\theta = \phi_{s,2}$. A plot of function $\rho_s(\theta)$ is shown in Figure 8.

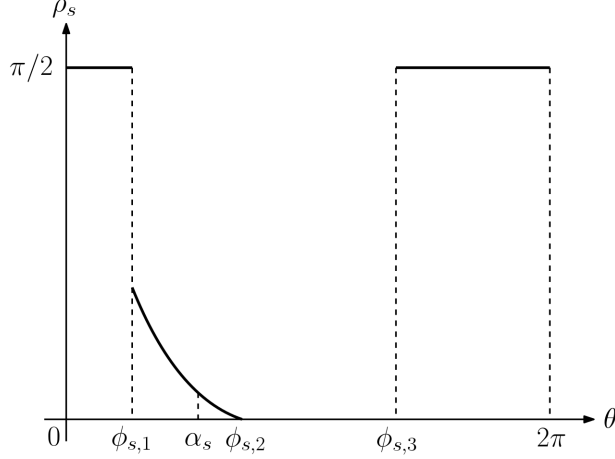


Figure 8: Illustration of function $\rho_s(\theta)$ in Case 1.

Case 2: s lies outside C_Π and inside C_Π' . For a line segment s lying outside C_Π and inside C_Π' , as depicted in Figure 9, we only need to worry about computing ρ_s for $\theta \in [\phi_{s,1}, \phi_{s,2}]$, given that $\rho_s = \pi/2$ for $\theta \in [0, \phi_{s,1}] \cup [\phi_{s,2}, 2\pi]$.

For $\theta \in [\phi_{s,1}, \phi_{s,2}]$, $\rho_s(\theta)$ is characterized by a piecewise continuous curve, which consists of at most two pieces, corresponding to sub-intervals $[\phi_{s,1}, \alpha_s]$ and $[\alpha_s, \phi_{s,2}]$, where α_s is the angle θ of the intersection point, if any, between C_Π and the supporting line of s . Note that if α_s exists, then $\rho_s(\theta)$ has two pieces; otherwise, $\rho_s(\theta)$ is constituted of one single piece.

Notice that $\phi_{s,2}$ is defined differently from the previous case. Here, $\phi_{s,2}$ is the largest θ at which the radius bc' of the quart-sector of θ intersects with s (at one of its endpoints). In fact, when $\theta = \phi_{s,2}$, $\rho_s(\theta) = \pi/2$. A plot of function $\rho_s(\theta)$ is shown in Figure 10.

Each of the curves $\rho_s(\theta)$ just described (for $\theta \in [\phi_{s,1}, \phi_{s,2}]$) is partially defined, continuous, and monotone over θ . Specifically, $\rho_s(\theta)$ is monotonically decreasing (resp. increasing) with respect to θ over the range of $[\phi_{s,1}, \phi_{s,2}]$ in Case 1 (resp. Case 2). In fact, the curves behave like pseudo-line segments, since any two curves can only intersect at most once.

Observe that $\rho_s(\theta)$ is an inverse trigonometric function. Nonetheless, we can define an algebraic function $f_s = \sin(\rho_s/2)$ in terms of variables x_b and y_b (i.e., x - and y -coordinates of $b \in C_\Pi$). The details of deriving f_s are presented next.

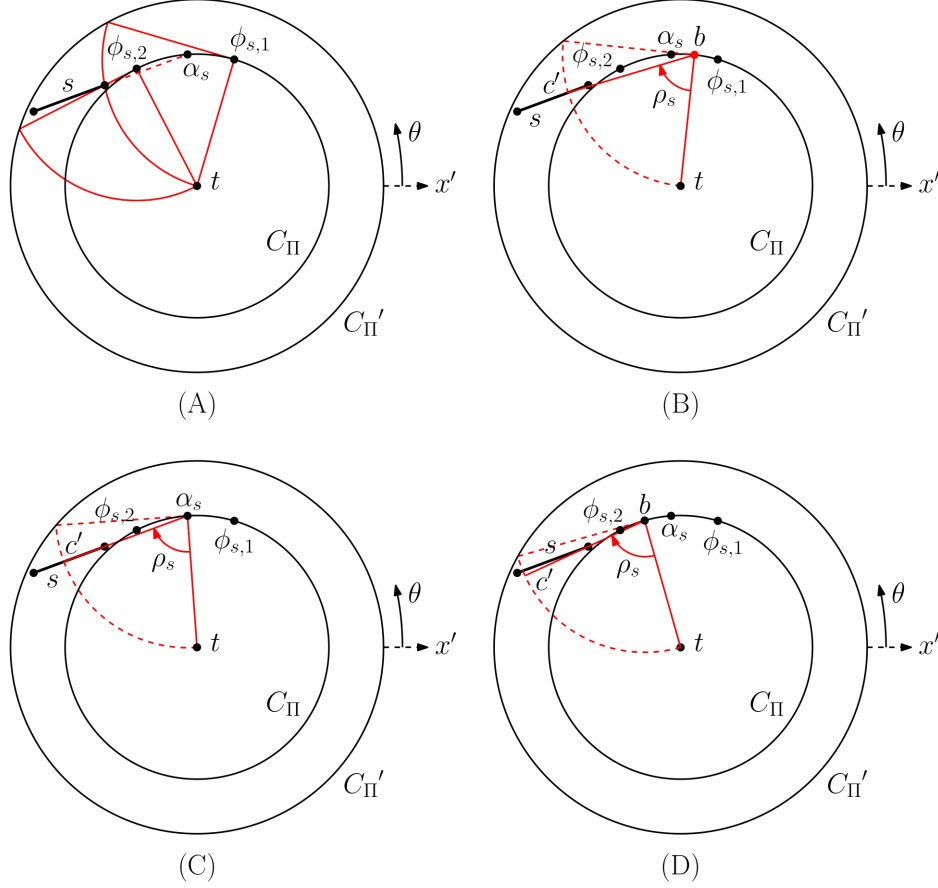


Figure 9: (A) Characterizing $\rho_s(\theta)$ for $\theta \in [\phi_{s,1}, \phi_{s,2}]$ in Case 2. Illustrations for $\rho_s(\theta)$ when (B) $\phi_{s,1} < \theta < \alpha_s$, (C) $\theta = \alpha_s$, and (D) $\alpha_s < \theta < \phi_{s,2}$, respectively.

Deriving algebraic function f_s . As one shall see, we can define an algebraic function f_s based on $\rho_s(\theta)$. Recall that, in Case 1, we are only concerned with characterizing $\rho_s(\theta)$ for $\theta \in [\phi_{s,1}, \phi_{s,2}]$, which consists of at most two pieces, corresponding to two sub-intervals $[\phi_{s,1}, \alpha_s]$ and $[\alpha_s, \phi_{s,2}]$. Let us consider the two sub-intervals individually. Note that, in the following analysis, θ is represented by the x - and y -coordinates of $b \in C_{\Pi}$ (in order to obtain an algebraic expression).

Sub-interval 1: $\theta \in [\phi_{s,1}, \alpha_s]$. For simplicity, let Π be the xy -plane (in which line segment s lies). Without loss of generality, let t be located at the origin. Let $x_{c'}$ and $y_{c'}$ denote the x - and y -coordinates of c' , respectively.

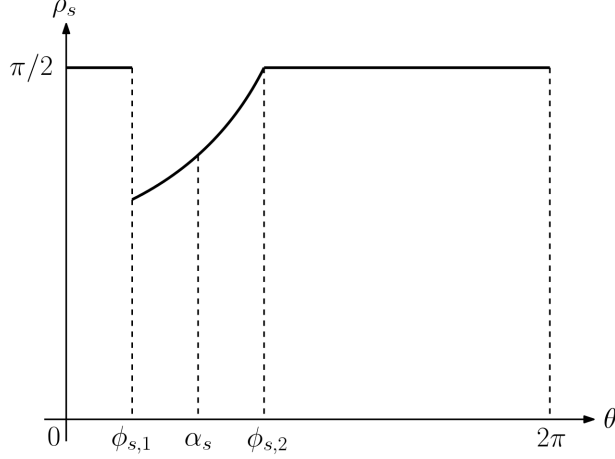


Figure 10: Illustration of function $\rho_s(\theta)$ in Case 2.

Observe that

$$\sin \frac{\rho_s}{2} = \frac{\sqrt{x_{c'}^2 + y_{c'}^2}}{2r} \quad (8)$$

Recall that c' is the intersection point between line segment s and the circle D_Π of radius r centered at b (see Figure 11). The coordinates of c' can be expressed in terms of the coordinates of b in the following manner. Let ℓ be the supporting line of s . Line ℓ can be represented by $y = mx + d$, where m is the slope of ℓ , and d is the y -intercept of ℓ . Circle D_Π can be formulated as $(x - x_b)^2 + (y - y_b)^2 = r^2$, where x_b and y_b are the x - and y -coordinates of b , respectively. Then, $x_{c'}$ and $y_{c'}$ can be written as

$$x_{c'} = \frac{x_b + y_b m + d m \pm \sqrt{\delta}}{1 + m^2} \quad (9)$$

$$y_{c'} = \frac{d + x_b m + y_b m^2 \pm \sqrt{\delta}}{1 + m^2} \quad (10)$$

where $\delta = r^2(1 + m^2) - (y_b - m x_b - d)^2$. Let $f_s = \sin(\rho_s/2)$ (i.e., Equation 8). Note that $f_s \in [0, \sqrt{1/2}]$. Clearly, by substituting Equations 9 and 10 into Equation 8, f_s can be expressed algebraically as a function of x_b and y_b , where $b \in C_\Pi$ and $x_b^2 + y_b^2 = r^2$.

Sub-interval 2: $\theta \in [\alpha_s, \phi_{s,2}]$. Observe that Equation 8 also holds true for this sub-interval. Let p be the intersection point between s and bc'

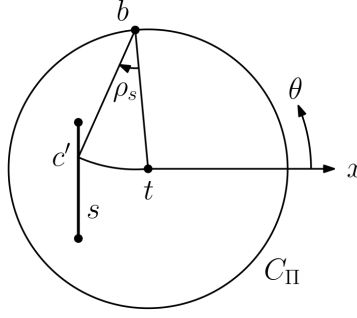


Figure 11: Case for $\theta \in [\phi_{s,1}, \alpha_s]$.

(see Figure 12). Note that p is an endpoint of s . Let x_p and y_p denote the x - and y -coordinates of p . Then, $x_{c'}$ and $y_{c'}$ can be expressed as

$$x_{c'} = x_b + \sqrt{\frac{r^2}{1 + \left(\frac{y_p - y_b}{x_p - x_b}\right)^2}} \quad (11)$$

$$y_{c'} = y_b + \sqrt{\frac{r^2}{1 + \left(\frac{y_p - x_b}{y_p - y_b}\right)^2}} \quad (12)$$

As before, we let $f_s = \sin(\rho_s/2)$, and f_s can be expressed algebraically as a function of x_b and y_b by substituting Equations 11 and 12 into Equation 8.

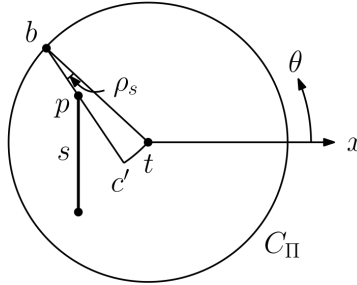


Figure 12: Case for $\theta \in [\alpha_s, \phi_{s,2}]$.

A similar derivation of f_s can also be performed in Case 2. Since ρ_s is partially defined, continuous, and monotone over $\theta \in [\phi_{s,1}, \phi_{s,2}]$, so must be function $f_s = \sin(\rho_s/2)$.

At this point, we are in position to claim a new unified data structure for solving the circular sector emptiness query problem in 2D. This \mathbb{R}^2 data structure simplifies the two-step approach described in [20] (which consists of a circular arc intersection query and a circular sector emptiness query) while having the same time and space complexity. Specifically, we construct two lower envelopes V_1 and V_2 of the piecewise algebraic curves f_s for all given line segments $s \in P$ as follows: V_1 is the lower envelope of the curves f_s for $y_b \geq 0$ (i.e., $0 \leq \theta \leq \pi$), whereas V_2 is for $y_b < 0$ (i.e., $\pi < \theta < 2\pi$). Note that V_1 and V_2 are computed as functions of x_b only, given that $y_b = +(r^2 - x_b^2)^{1/2}$ for $y_b \geq 0$, and $y_b = -(r^2 - x_b^2)^{1/2}$ for $y_b < 0$.

Since each pair of curves ρ_s intersect in at most one point, any two curves f_s do too. Thus, the size of the lower envelope is bounded by the third-order Davenport-Schinzel sequence, whose length is at most $O(n\alpha(n))$, where $\alpha(n)$ is the inverse Ackermann function. The lower envelope can be computed in $O(n \log n)$ time [10, 17].

Given a query circular sector σ , let b_σ be the apex of σ . If $y_{b_\sigma} \geq 0$, then x_{b_σ} is looked up in V_1 by using a binary search, which takes $O(\log n)$ time; otherwise, x_{b_σ} is looked up in V_2 . Let ρ be the acute angle between the two bounding radii of σ . If $\sin(\rho/2)$ is less than $f_s(x_b)$ for all line segments $s \in P$, then σ does not intersect P . Hence, we have the following result.

Theorem 3.2. *A set P of n line segments in \mathbb{R}^2 can be preprocessed in $O(n \log n)$ time into a data structure of size $O(n\alpha(n))$ so that, for a query circular sector σ with a fixed radius r and a fixed arc endpoint t , one can determine if σ intersects P in $O(\log n)$ time.*

As it turns out, we do not need to explicitly describe the function of the lower envelope. In fact, it suffices to have an implicit representation of the lower envelope – specifically, its vertices and the line segments that induce its various pieces. Generally, in order to obtain an implicit representation of the lower envelope (of a given set of curves), we require i) the number of times each pair of curves intersect, ii) the ability to compute the intersection points between any two given curves, and iii) the ability to determine whether one curve lies above or below another to the left and right of their intersection. Consider the following approach for computing an implicit representation of the lower envelope.

Computing implicit lower envelopes. We only address the case of computing V_1 ($0 \leq \theta \leq \pi$), and the other case of V_2 ($\pi < \theta < 2\pi$) can be handled

symmetrically. Recall that each pair of curves f_s intersect at most once. Thus, as with computing the lower envelope of a set of n line segments using a divide-and-conquer algorithm, we first sort the curves f_s by $\phi_{s,1}$. Note that, for a given line segment s , $\phi_{s,1}$ can be computed without knowing f_s , since $\phi_{s,1}$ corresponds to the smallest angle θ at which the circle of radius r centered at $b \in C_\Pi$ intersects with s . We divide the set of curves f_s into two equal sets by $\phi_{s,1}$, recursively compute the lower envelope of each set, and then merge the two lower envelopes to obtain the final result. The intersection of any two curves f_{s_i} and f_{s_j} (which correspond to line segments s_i and s_j , respectively) can be determined as follows. There are two cases to be considered, depending on how bc' is supported by s_i and s_j .

Case A. Line segment bc' intersects s_i and s_j at their endpoints (see Figure 13). Note that the corresponding x_b can be computed algebraically, given that b is the intersection point between C_Π and bc' . Specifically, C_Π can be represented as $x^2 + y^2 = r^2$. Let p and q denote the endpoints of s_i and s_j , respectively, that intersect bc' . Then, the line that passes through p and q can be expressed as $y = m_{pq}x + d_{pq}$, where $m_{pq} = (y_q - y_p)/(x_q - x_p)$ and $d_{pq} = y_p - [(y_q - y_p)/(x_q - x_p)]x_p$. Hence,

$$x_b = \frac{-d_{pq}m_{pq} \pm \sqrt{\delta_{pq}}}{1 + m_{pq}^2}$$

where $\delta_{pq} = r^2(1 + m_{pq}^2) - d_{pq}^2$. We can also decide in constant time (based on the slope of bc') which of the two curves f_{s_i} and f_{s_j} , to the left and right of their intersection at x_b , lies above/below the intersection point. For instance, in the example illustrated in Figure 13, we can easily determine that f_{s_j} lies below (resp. above) f_{s_i} to the left (resp. right) of their intersection at x_b .

Case B. Line segment bc' intersects s_i such that c' coincides with an interior point of s_i , and intersects s_j at its endpoint (see Figure 14). As with the previous case, we can compute the corresponding x_b algebraically. Let ℓ denote the supporting line of s_i , and let q be the intersection point between s_j and bc' . Line ℓ can be expressed as $y = m_\ell x + d_\ell$. Observe that the line passing through c' and q intersects C_Π at b ; let the line be represented as

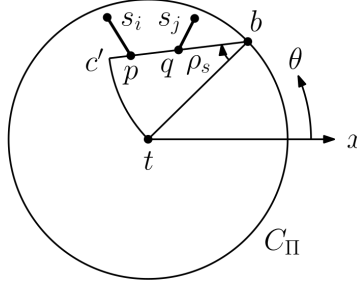


Figure 13: Case A.

$y = m_{c'q}x + d_{c'q}$. Then,

$$x_b = \frac{-d_{c'q}m_{c'q} \pm \sqrt{\delta_{c'q}}}{1 + m_{c'q}^2} \quad (13)$$

$$y_b = \frac{d_{c'q} \pm m_{c'q}\sqrt{\delta_{c'q}}}{1 + m_{c'q}^2} \quad (14)$$

where $m_{c'q} = (y_q - y_{c'})/(x_q - x_{c'})$, $d_{c'q} = y_{c'} - [(y_q - y_{c'})/(x_q - x_{c'})]x_{c'}$, and $\delta_{c'q} = r^2(1 + m_{c'q}^2) - d_{c'q}^2$. Since the circle of radius r centered at b intersects ℓ at c ,

$$x_{c'} = \frac{x_b + y_b m_\ell + d m_\ell \pm \sqrt{\delta_\ell}}{1 + m_\ell^2} \quad (15)$$

$$y_{c'} = \frac{d_\ell + x_b m_\ell + y_b m_\ell^2 \pm \sqrt{\delta_\ell}}{1 + m_\ell^2} \quad (16)$$

where $\delta_\ell = r^2(1 + m_\ell^2) - (y_b - m_\ell x_b - d_\ell)^2$. Clearly, we can determine x_b by using Equations 13–16. As before, we can also decide in $O(1)$ time which of the two curves f_{s_i} and f_{s_j} , to the left and right of their intersection at x_b , lies above/below the intersection point.

Notice that we did not compute a full (functional) description of the lower envelope. Instead, for each piece of the lower envelope, we store the information about the line segment s associated with the curve f_s to which the piece of the lower envelope belongs.

At query time, given a circular sector σ (and its associated x_b), we can determine if σ intersects any line segment in P , without having to know the equation for the curve f_s defining the lower envelope at x_b , as follows. We

Let G be the plane passing through points t and b . Plane G can be represented as $g_1x + g_2y + g_3z + g_4 = 0$, where $g_4 = 0$ and $g_3 = (-g_1x_b - g_2y_b)/z_b$. If we define $g = g_1/g_2$, then the expression for G becomes $gx + y + [(-g_1x_b - g_2y_b)/z_b]z = 0$. Given that G contains c' ,

$$gx_{c'} + y_{c'} + \left(\frac{-g_1x_b - g_2y_b}{z_b} \right) z_{c'} = 0 \quad (18)$$

Let H be the supporting plane of τ . Plane H can be expressed as $h_1x + h_2y + h_3z + h_4 = 0$, where h_1, h_2, h_3 , and h_4 are the known parameters determined based on the three vertices of τ . Since H contains c' ,

$$h_1x_{c'} + h_2y_{c'} + h_3z_{c'} + h_4 = 0 \quad (19)$$

Notice that $|bc'| = r$. Thus,

$$(x_{c'} - x_b)^2 + (y_{c'} - y_b)^2 + (z_{c'} - z_b)^2 = r^2 \quad (20)$$

Based on the three Equations 18, 19, and 20, we can obtain an algebraic expression for $x_{c'}$, $y_{c'}$, and $z_{c'}$, respectively, in terms of variables g , x_b , y_b , and z_b . By substituting the resulting algebraic expressions for $x_{c'}$, $y_{c'}$, and $z_{c'}$ into Equation 17, f_τ can be expressed algebraically as a function (of degree one) of g , x_b , y_b , and z_b , where $b \in C$ and $x_b^2 + y_b^2 + z_b^2 = r^2$.

Sub-interval 2: bc' intersects an edge of τ . Let s denote the edge of τ intersected by bc' . Edge s can be expressed in parametric form as

$$\begin{aligned} x &= (1 - \lambda_s)x_u + \lambda_s x_v \\ y &= (1 - \lambda_s)y_u + \lambda_s y_v \\ z &= (1 - \lambda_s)z_u + \lambda_s z_v \end{aligned}$$

where u and v are the two endpoints of s , and $0 \leq \lambda_s \leq 1$. Let p denote the intersection point between bc' and s . The supporting line ℓ of bc' can be represented as

$$\begin{aligned} x &= (1 - \lambda_\ell)x_b + \lambda_\ell x_p \\ y &= (1 - \lambda_\ell)y_b + \lambda_\ell y_p \\ z &= (1 - \lambda_\ell)z_b + \lambda_\ell z_p \end{aligned}$$

where $\lambda_\ell \in \mathbb{R}$. Given that p lies in s , and ℓ contains c' ,

$$x_{c'} = (1 - \lambda_\ell)x_b + \lambda_\ell[(1 - \lambda_s)x_u + \lambda_s x_v] \quad (21)$$

$$y_{c'} = (1 - \lambda_\ell)y_b + \lambda_\ell[(1 - \lambda_s)y_u + \lambda_s y_v] \quad (22)$$

$$z_{c'} = (1 - \lambda_\ell)z_b + \lambda_\ell[(1 - \lambda_s)z_u + \lambda_s z_v] \quad (23)$$

Note that Equation 20 still applies in this case. Substitute Equations 21, 22, and 23 into Equation 20, and solve for λ_ℓ in respect of variables λ_s , x_b , y_b , and z_b . Then, by substituting the resulting expression for λ_ℓ into Equations 21, 22, and 23, we obtain an algebraic expression (of degree one) for $x_{c'}$, $y_{c'}$, and $z_{c'}$, respectively, in terms of variables λ_s , x_b , y_b , and z_b .

At last, by substituting the algebraic expressions for $x_{c'}$, $y_{c'}$, and $z_{c'}$ into Equation (17), f_τ can be expressed algebraically as a function of λ_s , x_b , y_b , and z_b , where $b \in C$ and $x_b^2 + y_b^2 + z_b^2 = r^2$.

Finishing up. We construct two lower envelopes V_1 and V_2 of the piecewise algebraic functions f_τ for all given triangles $\tau \in P$, such that V_1 is the lower envelope of f_τ for $z_b \geq 0$, and V_2 is for $z_b < 0$. As a result, V_1 and V_2 are functions of only three variables.

For constructing the lower envelope of the trivariate piecewise algebraic functions (of constant description complexity) just described, the best-known performance bounds are given by Koltun [12] and Agarwal et al. [1]. Specifically, according to Koltun [12], we can compute the lower envelope deterministically in $O(n^{4+\epsilon})$ time and store it in a data structure of size $O(n^{4+\epsilon})$ and query time $O(\log n)$, for any $\epsilon > 0$. On the other hand, Agarwal et al. [1] showed that the lower envelope can be constructed in randomized expected time $O(n^{3+\epsilon})$ and stored in an $O(n^{3+\epsilon})$ -size data structure with a query time of $O(\log^2 n)$. Thus, we arrive at the result below.

Theorem 3.3. *For any constant $\epsilon > 0$, a set P of n triangles in \mathbb{R}^3 can be preprocessed in $O(n^{4+\epsilon})$ time into a data structure of size $O(n^{4+\epsilon})$ so that, for a query circular sector σ with a fixed radius r and an endpoint of its arc located at fixed point t , one can determine whether σ intersects P in $O(\log n)$ time.*

Given that $O(n^4)$ queries are to be processed in the worst case, the following result is obtained.

Lemma 3.4. *A feasible articulated probe trajectory, if one exists, can be determined in $O(n^{4+\epsilon})$ time using $O(n^{4+\epsilon})$ space, for any constant $\epsilon > 0$.*

Since the space/time complexity of finding an extremal feasible articulated trajectory (Lemma 3.4) is dominant over that of the case of unarticulated trajectory (Lemma 3.1), the final result can be stated as follows.

Theorem 3.5. *One can determine if a feasible trajectory exists, and if so, report (at least) one such trajectory in $O(n^{4+\epsilon})$ time using $O(n^{4+\epsilon})$ space, for any constant $\epsilon > 0$.*

As an alternative, an $O(n^5)$ -time algorithm with linear space usage is achievable by performing a simple $O(n)$ -check on each of the $O(n^4)$ extremal trajectories. The proposed enumeration algorithm is easy to implement and could be quite fast in practice, since the enumeration stops once a feasible solution is found. In addition, given that an extremal feasible probe trajectory amid n line segment obstacles in the plane can be obtained in $O(n^2)$ time [8], one could use a sampling-based method to find a feasible probe trajectory among n triangular obstacles in 3D space. Specifically, one could generate a finite set of planes passing through fixed point t either randomly or using an appropriate discretization scheme (i.e., with respect to parameters I and Ω), and then employ the existing data structure from [20] to compute the set of feasible trajectories, if any, in each plane.

4. Conclusion

We have presented efficient data structures and algorithms for solving a trajectory planning problem involving a simple articulated probe in 3D space. In particular, we have shown that a feasible probe trajectory, among n triangular obstacles, can be found in $O(n^{4+\epsilon})$ time, for any constant $\epsilon > 0$. In the process, we have solved a special case of the circular sector emptiness query problem in 3D and simplified the corresponding data structure in 2D. We leave open the following questions: 1) Since our approach is enumerative, can we speed up the process of finding one feasible solution? 2) Is it possible to extend the current algorithm to finding feasible probe trajectories of a given (or maximum) clearance?

Acknowledgment

The authors would like to thank Pankaj K. Agarwal for helpful discussions and comments.

References

- [1] Agarwal, P.K., Aronov, B., Sharir, M., 1997. Computing envelopes in four dimensions with applications. *SIAM Journal on Computing* 26, 1714–1732.
- [2] Agarwal, P.K., Matousek, J., 1994. On range searching with semialgebraic sets. *Discrete & Computational Geometry* 11, 393–418.
- [3] de Berg, M., Halperin, D., Overmars, M., Snoeyink, J., van Kreveld, M., 1994. Efficient ray shooting and hidden surface removal. *Algorithmica* 12, 30–53.
- [4] Biedl, T., Demaine, E., Demaine, M., Lazard, S., Lubiw, A., O’Rourke, J., Overmars, M., Robbins, S., Streinu, I., Toussaint, G., et al., 2001. Locked and unlocked polygonal chains in three dimensions. *Discrete & Computational Geometry* 26, 269–281.
- [5] Brooks, R.A., Lozano-Perez, T., 1985. A subdivision algorithm in configuration space for findpath with rotation. *IEEE Transactions on Systems, Man, and Cybernetics SMC-15*, 224–233.
- [6] Choset, H.M., Hutchinson, S., Lynch, K.M., Kantor, G., Burgard, W., Kavraki, L.E., Thrun, S., 2005. Principles of robot motion: theory, algorithms, and implementation. MIT Press.
- [7] Connelly, R., Demaine, E.D., 2017. Geometry and topology of polygonal linkages. *Handbook of Discrete and Computational Geometry*, 233–256.
- [8] Daescu, O., Teo, K.Y., 2020. Characterization and computation of feasible trajectories for an articulated probe with a variable-length end segment, in: 32nd Annual Canadian Conference on Computational Geometry.
- [9] Donald, B.R., 1984. Motion planning with six degrees of freedom. Technical Report. MIT Artificial Intelligence Lab.
- [10] Hershberger, J., 1989. Finding the upper envelope of n line segments in $O(n \log n)$ time. *Information Processing Letters* 33, 169–174.

- [11] Kavraki, L., Svestka, P., Latombe, J., Overmars, M., 1996. Probabilistic roadmaps for path planning in high-dimensional configuration spaces. *IEEE Transactions on Robotics and Automation* 12, 566–580.
- [12] Koltun, V., 2004. Almost tight upper bounds for vertical decompositions in four dimensions. *Journal of the ACM* 51, 699–730.
- [13] LaValle, S.M., 2006. *Planning algorithms*. Cambridge University Press.
- [14] LaValle, S.M., Kuffner Jr, J.J., 2001. Randomized kinodynamic planning. *The International Journal of Robotics Research* 20, 378–400.
- [15] McKenna, M., 1987. Worst-case optimal hidden-surface removal. *ACM Transactions on Graphics* 6, 19–28.
- [16] Pellegrini, M., 1993. Ray shooting on triangles in 3-space. *Algorithmica* 9, 471–494.
- [17] Sharir, M., Agarwal, P.K., 1995. *Davenport-Schinzel sequences and their geometric applications*. Cambridge University Press.
- [18] Sharir, M., Shaul, H., 2011. Semialgebraic range reporting and emptiness searching with applications. *SIAM Journal on Computing* 40, 1045–1074.
- [19] Simaan, N., Yasin, R.M., Wang, L., 2018. Medical technologies and challenges of robot-assisted minimally invasive intervention and diagnostics. *Annual Review of Control, Robotics, and Autonomous Systems* 1, 465–490.
- [20] Teo, K.Y., Daescu, O., Fox, K., 2020. Trajectory planning for an articulated probe. *Computational Geometry* , 101655.
- [21] Yakey, J.H., LaValle, S.M., Kavraki, L.E., 2001. Randomized path planning for linkages with closed kinematic chains. *IEEE Transactions on Robotics and Automation* 17, 951–958.
- [22] Zhu, D., Latombe, J., 1990. Constraint reformulation in a hierarchical path planner, in: *Proceedings of the IEEE International Conference on Robotics and Automation*, IEEE. pp. 1918–1923.